2020-08-15

Carbonate clumped isotope evidence for latitudinal seawater temperature gradients and the oxygen isotope composition of Early Cretaceous seas

Watanabe, Sayaka

10.1016/j.palaeo.2020.109777
Palaeogeography, Palaeoclimatology, Palaeoecology
Elsevier BV

Carbonate clumped isotope evidence for latitudinal seawater temperature gradients and the oxygen isotope composition of Early Cretaceous seas

Gregory D. Price[1]*, David Bajnai[2,3], Jens Fiebig[2]

[1] School of Geography, Earth & Environmental Sciences, University of Plymouth, Drake Circus, PL4 8AA Plymouth, UK

[2] Institute of Geosciences, Goethe University Frankfurt, Altenhöferalee 1, 60438 Frankfurt am Main, Germany

[3] Institute of Geology and Mineralogy, University of Cologne, Zülpicher Str. 49b, 50674 Cologne, Germany

*Corresponding author, email: g.price@plymouth.ac.uk, phone: +44 1752 584771

Keywords: thermometry, Valanginian, stable isotopes, belemnites

Abstract

In this study, we investigated Early Cretaceous (Valanginian, ca. 135 million years ago) climate from subtropical to boreal palaeolatitudes. Combined carbonate clumped isotope and oxygen isotope data derived from sub-arctic, boreal, and sub-tropical fossil belemnite rostra (Mollusca: Cephalopoda) provide new palaeotemperature estimates as well as a constraint on the oxygen isotope composition of seawater. Our belemnite data reveal balmy high-latitude marine temperatures (ca. 22 °C) and warm sub-tropical temperatures (ca. 31 °C). Supplementing our clumped isotope-based temperature estimates with published TEX_{86} data results in a conservative reconstruction of a latitudinal temperature gradient that is reduced compared to modern conditions. We find that modelling efforts are close to reproducing tropical temperatures when high pCO_2 levels are considered. Warm polar temperatures imply, however, that data-model discrepancies remain. Early Cretaceous seawater oxygen isotope values show a modern profile and are much more positive (up to 1.5‰ SMOW) than typically assumed. Based on our findings, if the positive Cretaceous seawater $\delta^{18}O$ values are not considered, carbonate $\delta^{18}O$ thermometry would underestimate temperatures, most acute at middle and tropical latitudes.

1 Introduction

Existing proxy data suggest that the Cretaceous latitudinal sea-surface temperature (SST) gradient was reduced (Barron, 1983; Naafs and Pancost, 2016; Littler et al., 2011; Voigt et al., 2003; Pucéat et al., 2003). The presence of extensive polar ice at this time, as suggested by Miller (2009) for example, is at odds with contemporaneous warm polar ocean temperatures, variable but high atmospheric CO_2 level (Berner and Kothavala, 2001; Wang et al., 2014; Witkowski et al., 2018) and the occurrence of tropical flora at mid- to high latitudes (Grasby et al., 2017). During much of the Cretaceous, stable oxygen isotope and TEX_{86} evidence suggests that equatorial surface waters were warmer (ca. 30–40 °C) and greater than the maximum SSTs recorded in the modern ocean (e.g. O'Brien et al., 2017; Huber et al., 2018). Mid to higher latitude surface waters were also 10–20 °C warmer than today (Naafs and Pancost, 2016; Littler et al., 2011; O'Brien et al., 2017; Huber et al., 1995; Jenkyns et al., 2012; Vickers et al., 2019; O'Connor et al., 2019).

The stable oxygen isotope composition ($\delta^{18}O$) of skeletal marine carbonates is perhaps the most widely used palaeotemperature proxy (Barron, 1983; Voigt et al., 2003; Pucéat et al., 2003; Huber et al., 2018; Mutterlose et al., 2012; Price et al., 2018). The challenge is, however, that the oxygen isotope composition of skeletal carbonates in marine systems vary as a function of both ambient temperatures and the oxygen isotope composition of seawater ($\delta^{18}O_{sw}$). Obtaining a value for $\delta^{18}O_{sw}$ is complicated because of variables that cannot be easily independently quantified, such as freshwater input, evaporation, and the extent of polar ice (Frakes and Francis, 1988; Price, 1999; Miller, 2009; Wierzbowski et al., 2018). Additionally, a proposed change in the mode of mid-ocean ridge hydrothermal alteration over tens of million year timescales suggests that the $\delta^{18}O_{sw}$ value has increased gradually through Earth's history, from ca. -6‰ SMOW in the Cambrian to its present value of ca. 0‰ SMOW (Standard Mean Ocean Water) (Veizer and Prokoph, 2015; Jaffrés et al., 2007). Nevertheless, the implied

climatic warmth, derived from the $\delta^{18}O$ values of skeletal marine carbonates, is consistent with more qualitative data derived from thermophilic floras and faunas from the high latitudes (Frakes and Francis, 1988; Tarduno, et al., 1998; Hurum et al., 2006; Spicer et al., 2008; Spicer and Herman 2010). However, Cretaceous General Circulation Model (GCM) simulations indicate that the latitudinal temperature gradient was much steeper than what the geological record suggests (Donnadieu et al., 2016; Lunt et al., 2016; Zhou et al., 2008; Poulsen et al., 2007).

The clumped isotope palaeothermometry technique measures the abundance of heavy (^{13}C–^{18}O bond bearing, mass 47) carbonate isotopologues within the single carbonate phase relative to its stochastic distribution, which is expressed as the Δ_{47} value. Clumped isotope-derived seawater temperatures are independent of the oxygen isotope composition of the waters (Ghosh et al., 2006). In this study, we analyse belemnite rostra (fossil remains of extinct marine cephalopods) using clumped isotope thermometry to provide new Δ_{47} data from the Early Cretaceous (Valanginian). Further, we examine equator-to-pole seawater temperature gradients and the $\delta^{18}O_{sw}$ values to aid temperature reconstructions and palaeoclimate modelling efforts.

2 Materials and methods

2.1 Stratigraphic and environmental setting

Belemnite rostra for this study were collected from four locations: the Khatanga Basin (Boyarka River, Russia, 70.592611° N, 97.369083° E), the Pechora Basin (Izhma River, Russia, 64.835150° N, 53.782200° E), the Cleveland Basin (Speeton, UK, 54.160555° N, 0.236111° W), and Caravaca (Southern Spain, 38.086944° N, 1.853889° W). These sites are spread across Tethyan, sub-Boreal, and Boreal locations, with palaeolatitudes ranging from 24° N to 74° N (Fig. 1).

The Lower Cretaceous part of the Boyarka River section is ca. 300 m thick and consists of marine sandstones, siltstones, and clays deposited in water depths of less than 100 m (Nunn et al., 2010). The fully marine macrofauna includes belemnites and ammonites, allowing a detailed Valanginian biostratigraphic zonation consistent with the Boreal biostratigraphic schemes (Fig. 2) and correlatable to Tethyan ammonite biostratigraphy (Nunn et al., 2010; Shulgina et al., 1994; Zakharov et al., 1997). Burial-history analysis of the Boyarka River region of the Khatanga Basin, suggests that a maximum burial depth is likely to be ca. 500 m and geothermal gradients to be moderate ca. 40 °C/km (Klett et al., 2011; Dobretsov et al., 2013).

The ca. 62-m-thick Izhma River section comprises shallow marine clastics with belemnites and ammonites present throughout. A detailed Berriasian (Ryazanian) to Valanginian biostratigraphic zonation is consistent with the Boreal biostratigraphic schemes and correlatable to Tethyan ammonite biostratigraphy (Nunn et al., 2010; Baraboshkin, 2004; Zakharov et al., 1997). Burial history curves suggest that the burial depth is likely to be no more than 1000 m, and the present thermal gradients in the Pechora Basin are moderate ca. 19–35 °C/km (Lindquist, 1999).

The Lower Cretaceous successions located near Caravaca, Southern Spain (Mai Valera, Sierra de Quipar, Canada Luenga) consist of nodular limestones with abundant marine fossils, including crinoid fragments, overlain by hemipelagic marl-limestone alternations (Aguado et al., 2000). The successions are thought to have been deposited in a low-energy marine basinal setting, with an estimated water depth of a few hundreds of meters (Company and Tavera, 2015). Here, the macrofauna consists mainly of belemnites and well-preserved ammonites, allowing detailed biostratigraphic zonation and correlation of the sections (Aguado et al., 2000; Janssen, 2003; Company and Tavera, 2015; Price, et al., 2018). The maturity of the organic matter in these Subbetic sections and other diagenetic observations imply that the burial depth

104 was no more than 1000 m and that the sediments never reached more than 80 °C (Reicherter
105 et al., 1996).
106 The Speeton Clay Formation of the Cleveland Basin comprises about 100 m of
107 interbedded shallow marine claystones deposited in water depths of less than 100 m. The
108 stratigraphical succession contains abundant belemnite rostra and well-preserved ammonites,
109 allowing detailed biostratigraphy (Rawson, 1973; McArthur et al., 2004) and correlation to
110 Boreal and Tethyan zonation schemes (Fig. 2). Measured $^{87}Sr/^{86}Sr$ values (McArthur et al., 2004)
111 show a good agreement between the biostratigraphic data. Vitrinite reflectance data collected
112 and analysed by Hemingway and Riddler (1982) for the Middle Jurassic, which lies beneath the
113 Speeton Clay Formation provides a temperature value of 95 °C for these Jurassic rocks. Holliday
114 (1999) took this information and assuming an average thermal conductivity provided a
115 geothermal gradient of approximately 30 °C/km and estimated maximum burial depths of ca.
116 2000 m. For the Cretaceous, the estimated sediment surface temperature used was 20 °C
117 (Holliday, 1999). These temperature estimates are consistent with the thermal history model
118 presented by Słowakiewicz et al. (2015) that suggests that the maximum temperatures for the
119 Lower Cretaceous succession reached ca. 40–50 °C during the early Cenozoic.
120 Theoretical calculations based on laboratory experiments evidence that solid-state
121 diffusion, even in wet and high-pressure conditions, is insignificant below 100 °C burial
122 temperatures on a timescale of 135 million years (Passey and Henkes 2012; Brenner et al.,
123 2018). Thus, the belemnite rostra analysed from these four sections should not have been
124 affected by solid-state reordering.
125
126 *2.2 Sample selection*
127 Belemnite rostra consist of diagenetically stable low-Mg calcite (Saelen, 1989). The
128 rostra selected for analysis in this study were those deemed to be the best-preserved samples

in the previous studies of McArthur et al. (2004), Nunn et al. (2010), Price et al. (2000), and Price et al. (2018). The excellent preservation of the analysed material is indicated by trace element concentrations and petrographic analyses, including cathodoluminescence. Diagenetic alteration of marine calcites often leads to significant enrichments in Mn and Fe (Veizer, 1974). Diagenetic Mn^{2+} ions are also an activator of orange cathodoluminescence in calcites, which is indicative of the alteration under reducing conditions (Marshall, 1992). All the belemnites analysed for clumped isotopes, in this study, had low concentrations of Fe (< 120 ppm) and Mn (< 25 ppm) indicative of good sample preservation (e.g. McArthur et al., 2007; Mutterlose et al., 2012). These 20 Valanginian belemnite rostra were: *Acroteuthis* sp. from Speeton from the Polyptychites Ammonite zone; *Berriasibelus*, *Hibolithes* and *Duvalia* from Caravaca from the Pertransiens–Verrucosum Ammonite zones; *Acroteuthis* and *Pachyteuthis* from Pechora Basin from the Klimovskiensis to Michalskii Ammonite zones, and *Acroteuthis, Lagonibelus* and *Pachyteuthis* from Khatanga Basin from the Klimovskiensis to Michalskii Ammonite zones schemes (Fig. 2). Calcite subsamples (ca. 50 mg carbonate powder) were taken from previously investigated rostra (see above), re-sampled across multiple growth bands, in order to get a representative amount for clumped isotope analysis. During sampling the belemnite rostra margins and calcite around the apical zones were avoided, as diagenetic alteration is typically observed in these parts. Visual inspection also showed belemnite rostra preservation to be excellent with all specimen displaying honey coloured translucent calcite. This is consistent with petrographic and cathodoluminescence observations (e.g. non-luminescent rostra) made in previous research (McArthur et al., 2004; Nunn et al., 2010; Price et al., 2000, 2018).

2.3 Clumped and stable isotope analyses

Clumped isotope analyses were performed using a ThermoFisher MAT 253 gas-source isotope-ratio mass spectrometer connected to an automated gas extraction and purification

line at the Institute of Geosciences, Goethe University Frankfurt. Carbonates were digested at 90 °C in a common acid bath. Background correction for the clumped isotope analyses was performed as described in Fiebig et al. (2016). Raw isotope values were calculated using the [*Brand*]/IUPAC set of isotopic parameters as suggested by Daëron et al. (2016). The raw Δ_{47} data were projected to the carbon dioxide equilibrium scale using empirical transfer functions that were determined using equilibrated gases (25 °C and 1000 °C, respectively) of various bulk isotope composition (Petersen et al., 2019). A 90–25 °C acid fractionation factor of 0.088‰ was applied to all $\Delta_{47\ (RFAC)}$ values (Petersen et al., 2019). To verify the consistency and precision of the clumped isotope measurements six carbonate standards were independently analysed along with the samples. The $\Delta_{47\ (RFAC)}$ (1 standard deviation, N = number of replicates) values of the reference material are: Carrara 0.407‰ (0.019‰, N = 335), MuStd 0.749‰ (0.018‰, N = 181), ETH 1 0.301‰ (0.016‰, N = 78), ETH 2 0.301‰ (0.019‰, N = 37), ETH 3 0.711‰ (0.018‰, N = 92), ETH 4 0.556‰ (0.020‰, N = 10) (Data S1). To convert $\Delta_{47\ (RFAC)}$ values to temperatures, we used a synthetic calcite calibration: $\Delta_{47\ (RFAC)} = 0.0383(\pm 1.7E\text{-}06) \times 10^6/T^2 + 0.258((\pm 1.7E\text{-}05)$ (Petersen et al., 2019), where T is in K and $\Delta_{47\ (RFAC)}$ is in ‰. $\delta^{18}O_{sw}$ estimates (Table 1, Data S1) were calculated using the Δ_{47}-derived temperature, the measured $\delta^{18}O$ value of each belemnite, and the $1000\ln\alpha_{calcite-water}$–temperature relationships of Kim and O'Neil (1997) (corrected for a CO_2-calcite acid fractionation factor of 10.25, Kim et al. (2007)) and of Coplen (2007). Coplen (2007) provided an equation based on water and vein calcite precipitated at extreme slow rates subaqueously at Devils Hole, Nevada, USA. The widely accepted Kim and O'Neil (1997) equation is based on inorganic precipitation experiments.

3 Results

3.1 Belemnite Δ_{47}-based temperatures

178 The average Δ_{47}-derived temperatures of this study range from 19 °C to 27 °C (Fig. 3,
179 Table 2, Supplementary Figure 1, Data S1). Some studies have postulated that belemnites
180 calcified their rostra, possibly seasonally, in the upper part of the water column (Klug et al.,
181 2016; Price et al., 2015; Stevens et al., 2014), whereas others consider belemnites as
182 nektobenthic organisms (Wierzbowski et al., 2013). For shallow marine settings (i.e. typically
183 less than 100 m), comparable to the locations investigated in this study (see above), one could
184 assume a low temperature gradient in the water column. Thus, here we presume that
185 belemnites indicate mean seawater temperatures at these sites at the time of rostra growth.
186 The range of Δ_{47}-derived temperatures encountered at each of the individual sample site was
187 from 4 °C to 15 °C. This relatively large temperature range is similar to that seen in other
188 clumped isotope studies (e.g. Petersen et al., 2016; Evans et al., 2018; Meyer et al., 2018). Such
189 a range in the Δ_{47}-derived temperature data is of a similar magnitude as the modern
190 temperature range (e.g. 4–12 °C) in similar latitudes (Locarnini et al., 2013) and is attributed to
191 a combination of the influence of seasonal temperature variability, different belemnite
192 ecologies combined with the impact of local geography and a reflection of the range of
193 temperature variability over the timescales represented by the belemnite sample set (see Fig.
194 2).
195 Our Δ_{47}-derived temperature estimate for the Valanginian low latitudes (27 °C) is lower
196 than the average temperature values of ca. 35 °C obtained from Valanginian TEX_{86}^{H} data (Littler
197 et al., 2011) but is comparable with modern mean annual surface temperature observations.
198 Our Δ_{47}-based temperatures suggest, therefore, that belemnites were calcifying their rostra in
199 waters slightly cooler than those surface waters indicated by the TEX_{86} data. Notably, the
200 belemnites from Caravaca occur in hemipelagic marly-limestone beds formed at a depth of a
201 few hundred meters (see above) and may have lived at times below a thermocline layer, so
202 their clumped isotope record may be subject to lower temperatures. Vickers et al. (2019) also

showed that Δ_{47}-derived palaeotemperatures were slightly cooler than TEX_{86}-based estimates. Multiple studies have now found that clumped temperatures of molluscs are always colder than TEX_{86}, temperature estimates, whether using the TEX_{86}^{H} or BAYSPAR TEX_{86} calibration. The temperature difference is commonly too great to be explained by surface vs. benthic modes of life alone (see Meyers et al., 2018). Despite the relatively large uncertainty in our temperatures estimates, our average Valanginian temperatures (19–24 °C) for the middle latitudes are warmer by up to 13 °C than other Valanginian temperature estimates derived from $\delta^{18}O$ thermometry of belemnites (Schootbrugge et al., 2000; Price et al., 2000; McArthur et al., 2004), although similar to Pucéat et al. (2003), who inferred temperatures from the oxygen isotope composition of fish tooth enamels. Our average Valanginian temperatures are also comparable to TEX_{86}^{H} data from other Cretaceous intervals (Mutterlose et al., 2010, 2012; Naafs and Pancost, 2016; O'Brien et al., 2017). For example, Mutterlose et al. (2012) suggest TEX_{86}^{H} seawater temperature estimates ranging from 22 °C to 24 °C for the Hauterivian of Speeton, UK. The temperature estimate for higher paleolatitudes (74° N) from this study is 19 °C and is warmer than previous Valanginian carbonate $\delta^{18}O$-based estimates (Price and Nunn, 2010; Ditchfield, 1997) but similar to Late Cretaceous TEX_{86}^{H} seawater temperature estimates (Super et al., 2018). Different calibrations have been proposed to translate TEX_{86} into SST. Of these calibrations, the global nonlinear logarithmic TEX_{86}^{H} calibration of Kim et al. (2010) and the BAYSPAR TEX_{86} calibration of Tierney and Tingley (2014) are the most commonly chosen for higher-temperature settings, such as in the Cretaceous. It is the more conservative TEX_{86}^{H} estimates that provide a better match to our clumped isotope temperature estimates (see also Vickers et al., 2019). The BAYSPAR TEX_{86} calibration of Tierney and Tingley (2014) provides higher temperatures (ca. 8 °C higher) at the upper limit of the proxy (e.g. O'Brien et al. 2017; O'Connor et al., 2019). Our Valanginian seawater temperatures across all latitudes are

also 1–14 °C warmer than modern SST observations, although at middle latitudes, they approach the warmest recent observations (Locarnini et al., 2013).

The interpretation of relatively warm past ocean temperatures at middle-high latitudes is consistent with palaeobotanical temperature constraints derived from Cretaceous fossil floras (Spicer and Herman, 2010). In contrast, data from the Lower Cretaceous of Canada (Grasby et al., 2017), Svalbard (Vickers et al., 2016), and Siberia (Rogov et al., 2017) suggest that numerous boreal cool events interrupted otherwise warm conditions. These authors describe abundant glendonites (pseudomorphs after marine sedimentary ikaite) in Valanginian and Aptian strata that are thought to be critical markers of cold conditions. These observations are not incompatible with our data from the Valanginian, as Grasby et al. (2017) conclude that cold periods were brief, punctuating an overall warm Early Cretaceous climate.

4 Discussion

4.1 Early Cretaceous latitudinal temperature gradient

Using the average palaeotemperatures and the palaeolatitude (Young et al., 2019) at each of the sites examined here, together with Valanginian Δ_{47} data from Price and Passey (2013) and TEX_{86} data from Littler et al. (2011), we can conservatively reconstruct an Early Cretaceous latitudinal temperature profile with an estimated gradient of ca. 0.32 °C per degree of latitude, between 15° N and 74° N (Fig. 3). TEX_{86} data from other Early Cretaceous intervals (Naafs and Pancost, 2016) and Late Cretaceous $\delta^{18}O$-derived palaeotemperatures (Voigt et al., 2003; Pucéat et al., 2003) also reveal a similar gradient. Available TEX_{86} data evidence (O'Brien et al. 2017; O'Connor et al., 2019) suggests that latitudinal temperature gradients were lower in the Coniacian to Campanian compared with the present day. The implied shallow meridional temperature gradient for the Early Cretaceous contrasts with a modern average gradient of ca. 0.45 °C per degree of latitude in the Northern Hemisphere (Young et al., 2019).

Most evidence suggests that the Cretaceous was characterised by high atmospheric CO_2 levels (e.g. Berner and Kothavala, 2001; Wang et al., 2014; Witkowski et al., 2018) and consequently, its climate was warmer and more equable (Frakes 1979; Huber et al., 1995; Bice et al., 2003). Although, as noted above, transient cool events have been suggested (Grasby et al., 2017; Mutterlose et al., 2010; McArthur et al., 2007), data typically point to warm polar regions (Spicer and Herman, 2010; Ditchfield 1997; Frakes, 1979; McArthur et al., 2007) consistent with our temperature estimates. The presence of such a reduced temperature gradient requires a climate mechanism in a high pCO_2-world that yields temperate polar regions while not overheating the tropics. Proposed mechanisms to increase the transfer of heat toward the poles include increased oceanic (Schmidt and Mysak, 1996) and atmospheric poleward heat transport (Bice et al., 2003), together with amplification of polar warmth by cloud feedbacks (Kump and Pollard 2008; Sagoo et al., 2013; Upchurch et al., 2015).

4.2 Cretaceous model-data comparisons

Climate modelling of past warm periods has received much attention as it has long been suggested that simulations may not capture the extent to which the latitudinal temperature gradient is reduced (Spicer, et al., 2008). The Δ_{47} reconstructions and temperature compilation demonstrate that Early Cretaceous tropical warming was of a magnitude consistent with some models (e.g. using the fast ocean atmosphere model (FOAM), for the Late Cretaceous, Donnadieu et al., 2016) at 12-times pre-industrial pCO_2 (Fig. 3). Other simulations indicate cooler tropical temperatures. For example, modelled Valanginian sea surface temperatures (using the UK Met Office HadCM3L model) with 4x pre-industrial pCO_2 (Lunt et al., 2016) shows less of a fit particularly with the Littler et al. (2011) TEX_{86} temperature data, which represents the sea surface, as does the model. For higher latitudes, our temperature proxy data are warmer than some simulations (Donnadieu et al., 2016; Lunt et al., 2016; Poulsen et al., 2007;

277 Upchurch et al., 2015) for the Early and Late Cretaceous even at 12-times pre-industrial pCO_2.
278 In contrast to these Cretaceous simulations, climate models of other "greenhouse" intervals
279 (e.g. for the Eocene, Sagoo et al., 2013; Zhu et al., 2019), show warmer higher latitudes.
280 Although many aspects contributed to the warmth seen at higher latitudes in the model of
281 Sagoo et al., (2013), a strong sensitivity to albedo changes associated with cloud cover was
282 apparent. However, for the highest latitude proxy data, the magnitude of warming simulated
283 by most climate models is still less than indicated by the Δ_{47} data and published TEX_{86} (Jenkyns
284 et al., 2012) temperature estimates. This could suggest that some climate models for the
285 Cretaceous are still missing key processes. Notably, Upchurch et al. (2015) using a fully coupled
286 GCM come close to reproduce warm Cretaceous polar temperatures and the latitudinal
287 temperature gradient without overheating the tropics. For a cool greenhouse interval of the
288 latest Cretaceous (Maastrichtian) the best fits of Upchurch et al. (2015) for mean annual
289 temperature are simulations that use 6-times pre-industrial levels of atmospheric CO_2, or 2-
290 times pre-industrial levels of atmospheric CO_2 and liquid cloud properties that may reflect pre-
291 anthropogenic levels of cloud condensation nuclei. It is important to note that Cretaceous TEX_{86}
292 data and Δ_{47}-derived temperatures are limited by the distribution of suitably preserved
293 sediments at high latitudes. Indeed, Cretaceous TEX_{86} data is available from just a few Arctic
294 sites (Jenkyns et al., 2004; Super et al., 2018). As such, the high temperatures so far identified
295 may not be fully representative of regional averages.
296
297 *4.3 The oxygen isotope composition of Early Cretaceous seas*
298 Estimations of ancient oceans $\delta^{18}O_{sw}$ values are controversial. Complexity arises from
299 variables such as the input of freshwater and evaporation, the presence or absence of polar ice,
300 whether the oxygen isotope composition of the seawater is buffered by submarine
301 hydrothermal processes, or whether lower $\delta^{18}O$ values of ancient marine carbonates reflect the

fact that the $\delta^{18}O_{sw}$ value has varied significantly over time (see Jaffrés et al., 2007). The average of our $\delta^{18}O_{sw}$ estimates is calculated as -0.1‰ SMOW using the Coplen (2007) equation or 1.4‰ SMOW using the Kim and O'Neil (1997) equation (Table 2, Data S1). Both values are more positive than the estimated global average $\delta^{18}O_{sw}$ value for the modern ocean (-0.28‰ SMOW) or an ice-free world (-1.0‰ SMOW) (Shackleton and Kennett, 1975) (Fig. 4). The $\delta^{18}O_{sw}$ value of -1.0‰ SMOW is widely cited as the mean seawater oxygen isotope composition for the Cretaceous. Nevertheless, our data from four new sites, in conjunction with data from Price and Passey (2013), suggests a gentle decrease in average values poleward (Fig. 4, Supplementary Figure 2) (see also Zhou et al., 2008). The difference between our calculated $\delta^{18}O_{sw}$ values and modern $\delta^{18}O_{sw}$ values, or the assumed $\delta^{18}O_{sw}$ values for ancient seas in ice-free hothouse worlds, may be due to (1) differences in the absolute Δ_{47}-temperature calibration producing temperatures that are too warm, (2) vital effects in the belemnites resulting in carbonate $\delta^{18}O$ values enriched relative to equilibrium with seawater, (3) diagenesis causing lower Δ_{47} and higher $\delta^{18}O$ values in carbonates, or (4) changes in $\delta^{18}O_{sw}$ values of ancient seas.

Differences in the Δ_{47}-temperature calibration would influence absolute temperature and calculated $\delta^{18}O_{sw}$ values. As noted above, we used the synthetic Δ_{47}–temperature calibration of Petersen et al. (2019) to convert the measured clumped isotope values to precipitation temperatures of calcium carbonate. This calibration is fairly robust as it considers 451 carbonate datapoints. In comparison, the in-house Wacker et al. (2014) or the steeper sloped Kelson et al. (2017) calibrations give temperatures that are ca. 3 °C warmer (Data S1). Hence our choice of calibration eliminates potential biasing towards too warm temperatures.

Alternatively, the high $\delta^{18}O_{sw}$ values could be caused by diagenetic effects that increased temperatures. Modelling of burial at all sites suggests that the belemnite rostra analysed should not have been affected by solid-state reordering. Alternatively, the high $\delta^{18}O_{sw}$ values may be due to vital effects. Should Kim and O'Neil (1997) represent equilibrium, then

our mean $\delta^{18}O_{sw}$ value would be on average 2.4‰ higher than the value assumed for an ice-free ocean (see below). Kinetic isotope effects generally, however, discriminate against the heavier isotope (e.g. McConnaughey 1989), although Price et al. (2015) do suggest a possible offset between belemnite calcite $\delta^{18}O$ and equilibrium of ca. 1‰. Data from a number of other Cretaceous studies applying the clumped isotope palaeothermometer to molluscs (Dennis et al., 2013; Meyer et al., 2018; Vickers et al., 2019), also indicates that the isotopic composition of seawater predicted was markedly positive, using the equation of Kim and O'Neil (1997) and exceeding modern seawater values. Further work comparing the clumped isotope temperatures to different molluscs (see Meyer et al. 2018) could resolve whether these high $\delta^{18}O_{sw}$ values could be caused by vital effects.

In addition to those studies noted above, data from a number of other studies applying the clumped isotope palaeothermometer (Petersen and Schrag 2015; Wierzbowski et al 2018), also note that the isotopic composition of seawater predicted was, at times, markedly positive. This poses a challenge, as the average value of modern $\delta^{18}O_{sw}$ is a consequence of ice accumulation largely on Greenland and Antarctica. Although modest-sized Cretaceous ice sheets have been postulated (DeConto and Pollard, 2003; Frakes and Francis, 1988; Price, 1999), the volume of this ice is likely to be insufficient to see $\delta^{18}O_{sw}$ values around 1‰ SMOW. $\delta^{18}O_{sw}$ values of 1‰ SMOW require ice volumes in excess of the Last Glacial Maximum, when ice sheets covered large parts of North America and Europe as well as Antarctica. Unlike at the Last Glacial Maximum, it is thought that in the Cretaceous, ice was considerably more limited and is, therefore, not sufficient to explain such high $\delta^{18}O_{sw}$ values. Any ice would also have to be isotopically very light. Studies have also postulated that water could be stored as (isotopically light) freshwater on land (e.g. Jacobs and Sahagian, 1993). As this study, however, suggests that the latitudinal temperature gradient during the Early Cretaceous was less steep than today, it is conceivable that the $\delta^{18}O_{ice}$ and any stored freshwater was also less extreme. If

352 the $\delta^{18}O_{ice}$ value was less negative, this would make it even harder to get $\delta^{18}O_{sw}$ values to 1‰
353 SMOW or more, as even greater ice volumes would be required. This is consistent with studies
354 of the Antarctic ice sheet during the early Miocene when the latitudinal temperature gradient
355 was less extreme and Antarctic temperatures were warmer than today resulting in significantly
356 higher $\delta^{18}O_{ice}$ values in the Miocene ice sheet (e.g. ca. -35‰ SMOW) than values today
357 (i.e. -45‰ to -55‰ SMOW) (Pekar and DeConto, 2006).

358 Alternatively, the high $\delta^{18}O_{sw}$ values could be caused by relatively high rates of
359 evaporation leading to higher salinities. Although, salinity can be estimated from salinity–$\delta^{18}O$
360 models for marine basins (e.g. Railsback et al., 1989), to reconcile our belemnite $\delta^{18}O$ data with
361 the Δ_{47}-derived temperatures, salinities in excess of 41 PSU are required (see also Wierzbowski
362 et al., 2018). As such, each of the sites examined here would need to be dominated by
363 evaporation. As the belemnite samples were derived from open marine systems (based upon
364 the presence of a fully marine fauna, including ammonites), high salinities contributing to high
365 $\delta^{18}O_{sw}$ values seems unlikely.

366 The marine carbonate $\delta^{18}O$ record also depends on seawater pH (Wallmann, 2004).
367 Seawater pH is strongly influenced by changes in pCO_2 (Zeebe, 1999, 2001; Wallmann, 2004).
368 An increase of seawater pH of 0.2–0.3 units, for example, is considered to result in a decrease
369 of about 0.22–0.33‰ in the $\delta^{18}O$ values of foraminiferal calcite, which would normally be
370 interpreted as a temperature increase of seawater, although the magnitude of the effect may
371 be species-dependent (Zeebe, 2001). During periods of high atmospheric CO_2 levels such as the
372 Cretaceous (Berner and Kothavala, 2001; Wang et al., 2014; Witkowski et al., 2018), this pH
373 effect (Zeebe, 2001) if applicable to belemnites, would lead to an increase in the $\delta^{18}O$ value of
374 calcite. However, the magnitude of pH change in seawater needed to explain the observed
375 offset in $\delta^{18}O_{sw}$ value between an ice-free -1‰ SMOW and the average of our estimate of
376 +1.5‰ SMOW (using the Kim and O'Neil, 1997 equation) and scaling of ca. 0.1 pH unit for every

0.1‰ $\delta^{18}O$, means that oceans would need to be ca. 2.5 pH units more acidic. Such a magnitude of change is not realistic (see Caldeira and Wickett, 2003).

Changes in the oxygen isotope composition of ancient oceans is a debated issue. Veizer and Prokoph (2015) and Jaffrés et al. (2007) for example suggest that the $\delta^{18}O_{sw}$ value has increased gradually through Earth's history, from -6‰ SMOW in the Cambrian to its present value of ca. 0‰ SMOW. Other studies, applying the clumped isotope palaeothermometer, indicate more or less constant $\delta^{18}O_{sw}$ values through geologic time (e.g. Ryb and Eiler, 2018; Henkes, et al., 2018). Most models of the geological ^{18}O-cycle conclude that seawater/rock interaction with silicates of oceanic crust at high and low temperatures balance each other and, thus buffer the $\delta^{18}O_{sw}$ value at about 0(±2)‰ SMOW (Muehlenbachs and Clayton, 1976; Holland, 1984). Hence, it has been considered that the $\delta^{18}O_{sw}$ value of the global ocean has not changed significantly over time, but has been buffered by hydrothermal and weathering processes (low-temperature interactions with silicates) at mid-ocean ridges and on ridge flanks, based on results of ophiolite studies (e.g. Coogan et al., 2019). High-temperature alteration (mainly via hydrothermal fluids) leads to an increase in $\delta^{18}O_{sw}$ values, while low-temperature alteration (e.g. weathering processes) leave the ocean ^{18}O-depleted (Muehlenbachs and Clayton, 1976; Holland, 1984; Muehlenbachs, 1998). These mass balance calculations, however, do not rule out minor variations in the average $\delta^{18}O_{sw}$ value that could conceivably produce a minor change towards more positive values reconciling our belemnite $\delta^{18}O$ data and corresponding Δ_{47}-derived temperatures.

5 Conclusions

The Early Cretaceous Δ_{47}-derived temperatures of this study point to Arctic regions above freezing. Our data argue against an extended ice sheet in the Northern Hemisphere and shows congruence with TEX_{86} temperatures. Our clumped isotope-based temperature reconstruction suggests the existence of a strongly reduced equator-to-pole temperature

gradient in the Northern Hemisphere. We find that modelling efforts are close to reproducing the tropical temperatures when high atmospheric CO_2 levels are invoked, however, our data suggests warmer temperatures at higher latitudes that are not shown in the models.

The results of this study indicate that it is unlikely that the oxygen isotope composition of the seawater was homogenous. Our Early Cretaceous $\delta^{18}O_{sw}$ results are a conservative reconstruction of a latitudinal gradient that shows a gentle decrease in values poleward and also, using the Kim and O'Neil (1997) and Coplen (2007) equations plot in the upper portion or wholly within the field of modern seawater. Early Cretaceous $\delta^{18}O_{sw}$ values with modern characteristics implies some storage of light isotopes away from the ocean, e.g. as ice accumulation on Antarctica. The constraints we provide on the oxygen isotope composition of Early Cretaceous seawater, underpins our understanding of the evolution of the Earth's temperature. Disregarding positive Early Cretaceous $\delta^{18}O_{sw}$ values results in an underestimation of temperatures, most acute at middle and tropical latitudes.

Acknowledgements

Funding for this study was provided by a UK Natural Environment Research Council (NERC) grant (NE/J020842/1) to GDP. We thank S. Hofmann, C. Schreiber (Goethe University Frankfurt), N. Löffler, K. Methner and E. Krsnik (Senckenberg BIK-F) for their technical help. Further supporting data can be accessed in Table 1 of Supporting information. The authors declare no conflicts of interest. We would like to thank reviewers Sierra Petersen and Hubert Wierzbowski for comprehensive and constructive reviews that greatly improved the manuscript. Comments from Thomas Algeo also improved the manuscript. Further supporting data can be accessed in the Supporting information and on Pangaea (https://doi.pangaea.de/10.1594/PANGAEA.907273)

References

Aguado, R., Company, M., Tavera, J.M., 2000. The Berriasian/Valanginian boundary in the Mediterranean region: New data from the Caravaca and Cehegín sections, SE Spain. Cretac. Res. 21, 1-21. https://doi.org/10.1006/cres.2000.0198

Baraboshkin, E.Y., 2004. Boreal-Tethyan correlation of Lower Cretaceous ammonite scales. Moscow Univ. Geol. Bull. 59, 9-20.

Barron, E.J., 1983. A warm, equable Cretaceous: The nature of the problem. Earth-Sci. Rev. 19, 305-338. https://doi.org/10.1016/0012-8252(83)90001-6

Berner, R.A., Kothavala, Z., 2001. GEOCARB III: A revised model of atmospheric CO_2 over phanerozoic time. Am. J. Sci. 301, 182-204. https://doi.org/10.2475/ajs.301.2.182

Bice, K.L., Huber, B.T., Norris, R.D., 2003. Extreme polar warmth during the Cretaceous greenhouse? Paradox of the late Turonian $\delta^{18}O$ record at Deep Sea Drilling Project Site 511. Paleoceanography 18, 1031. https://doi.org/10.1029/2002pa000848

Brenner, D.C., Passey, B.H., Stolper, D.A., 2018. Influence of water on clumped-isotope bond reordering kinetics in calcite. Geochim. Cosmochim. Acta 224, 42-63. https://doi.org/10.1016/j.gca.2017.12.026

Caldeira, K., Wickett, M.E., 2003. Oceanography: Anthropogenic carbon and ocean pH. Nature 425, 365. https://doi.org/10.1038/425365a

Company, M., Tavera, J.M., 2015. Lower Valanginian ammonite biostratigraphy in the Subbetic Domain (Betic Cordillera, southeastern Spain). Carnets Geol. 15, 71-88.

Coogan, L.A., Daëron, M., Gillis, K.M., 2019. Seafloor weathering and the oxygen isotope ratio in seawater: Insight from whole-rock $\delta^{18}O$ and carbonate $\delta^{18}O$ and Δ_{47} from the Troodos ophiolite. Earth Planet. Sci. Lett. 508, 41-50. https://doi.org/10.1016/j.epsl.2018.12.014

Coplen, T.B., 2007. Calibration of the calcite–water oxygen-isotope geothermometer at Devils Hole, Nevada, a natural laboratory. Geochim. Cosmochim. Acta 71, 3948-3957. https://doi.org/10.1016/j.gca.2007.05.028

Daëron, M., Blamart, D., Peral, M., Affek, H.P., 2016. Absolute isotopic abundance ratios and the accuracy of Δ_{47} measurements. Chem. Geol. 442, 83-96. https://doi.org/10.1016/j.chemgeo.2016.08.014

DeConto, R.M., Pollard, D., 2003. Rapid Cenozoic glaciation of Antarctica induced by declining atmospheric CO_2. Nature 421, 245-249. https://doi.org/10.1038/nature01290

Dennis, K.J., Cochran, J.K., Landman, N.H., Schrag, D.P., 2013. The climate of the Late Cretaceous: New insights from the application of the carbonate clumped isotope thermometer to Western Interior Seaway macrofossil. Earth Planet. Sci. Lett. 362, 51-65. https://doi.org/10.1016/j.epsl.2012.11.036

Ditchfield, P.W., 1997. High northern palaeolatitude Jurassic-Cretaceous palaeotemperature variation: new data from Kong Karls Land, Svalbard. Palaeogeogr. Palaeoclimatol. Palaeoecol. 130, 163-175. https://doi.org/10.1016/S0031-0182(96)00054-5

Dobretsov, N.L., Polyansky, O.P., Reverdatto, V.V., Babichev, A.V., 2013. Dynamics of the Arctic and adjacent petroleum basins: a record of plume and rifting activity. Russ. Geol. Geophys. 54, 888-902. https://doi.org/10.1016/j.rgg.2013.07.009

Donnadieu, Y., Puceat, E., Moiroud, M., Guillocheau, F., Deconinck, J.F., 2016. A better-ventilated ocean triggered by Late Cretaceous changes in continental configuration. Nat. Commun. 7, 10316. https://doi.org/10.1038/ncomms10316

Evans, D., Sagoo, N., Renema, W., Cotton, L.J., Müller, W., Todd, J.A., Saraswati, P.K., Stassen, P., Ziegler, M., Pearson, P.N., Valdes, P.J., Affek, H.P., 2018. Eocene greenhouse climate revealed by coupled clumped isotope-Mg/Ca thermometry. Proc. Natl. Acad. Sci. U.S.A. 115, 1174-1179. https://doi.org/10.1073/pnas.1714744115

Fiebig, J., Hofmann, S., Niklas, L., Lüdecke, T., Methner, K., Wacker, U., 2016. Slight pressure imbalances can affect accuracy and precision of dual inlet-based clumped isotope analysis. Isotopes Environ. Health Stud. 52, 12-28. https://doi.org/10.1080/10256016.2015.1010531

Frakes, L.A., 1979. Climates throughout geologic time. Elsevier, Amsterdam.

Frakes, L.A., Francis, J.E., 1988. A guide to Phanerozoic cold polar climates from high-latitude ice-rafting in the Cretaceous. Nature 333, 547-549. https://doi.org/10.1038/333547a0

Ghosh, P., Adkins, J., Affek, H., Balta, B., Guo, W., Schauble, E.A., Schrag, D., Eiler, J.M., 2006. ^{13}C–^{18}O bonds in carbonate minerals: A new kind of paleothermometer. Geochim. Cosmochim. Acta 70, 1439-1456. https://doi.org/10.1016/j.gca.2005.11.014

Gradstein, F.M., Ogg, J.G., Schmitz, M.D., Ogg, G.M., 2012. The Geologic Time Scale 2012. Elsevier, p. 1176.

Grasby, S.E., McCune, G.E., Beauchamp, B., Galloway, J.M., 2017. Lower Cretaceous cold snaps led to widespread glendonite occurrences in the Sverdrup Basin, Canadian High Arctic. Geol. Soc. Am. Bull. 129, 771-787. https://doi.org/10.1130/B31600.1

Hemingway, J.E., Riddler, G.P., 1982. Basin inversion in North Yorkshire. T. I. Min. Metall. B 91, B175-B186.

Henkes, G.A., Passey, B.H., Wanamaker, A.D., Grossman, E.L., Ambrose, W.G., Carroll, M.L., 2013. Carbonate clumped isotope compositions of modern marine mollusk and brachiopod shells. Geochim. Cosmochim. Acta 106, 307-325. https://doi.org/10.1016/j.gca.2012.12.020

Henkes, G.A., Passey, B.H., Grossman, E.L., Shenton, B.J., Yancey, T.E., Pérez-Huerta, A., 2018. Temperature evolution and the oxygen isotope composition of Phanerozoic oceans from carbonate clumped isotope thermometry. Earth Planet. Sci. Lett. 490, 40-50. https://doi.org/10.1016/j.epsl.2018.02.001

500 Holland, H.D., 2004. The geologic history of seawater, in: Elderfield, H., Holland, H.D., Turekian,
501 K.K. (Eds.), Treatise on Geochemistry, Vol. 6. The Oceans and Marine Geochemistry.
502 Elsevier Pergamon, Kidlington, Oxford, pp. 583–625.
503 Holliday, D.W., 1999. Palaeotemperatures, thermal modelling and depth of burial studies in
504 northern and eastern England. Proc. Yorkshire Geol. Soc. 52, 337-352.
505 https://doi.org/10.1144/pygs.52.4.337
506 Huber, B.T., Hodell, D.A., Hamilton, C.P., 1995. Middle-Late Cretaceous climate of the southern
507 high latitudes: Stable isotopic evidence for minimal equator-to-pole thermal gradients.
508 Geol. Soc. Am. Bull. 107, 1164-1191. https://doi.org/10.1130/0016-
509 7606(1995)107<1164:MLCCOT>2.3.CO;2
510 Huber, B.T., MacLeod, K.G., Watkins, D.K., Coffin, M.F., 2018. The rise and fall of the Cretaceous
511 hot greenhouse climate. Glob. Planet. Change 167, 1-23.
512 https://doi.org/10.1016/j.gloplacha.2018.04.004
513 Hurum, J.H., Milan, J., Hammer, O., Midtkandal, I., Amundsen, H., Saether, B., 2006. Tracking
514 polar dinosaurs - new finds from the Lower Cretaceous of Svalbard. Norw. J. Geol. 86,
515 397-402.
516 Jacobs, D.K., Sahagian, D.L., 1993. Climate-induced fluctuations in sea level during non-glacial
517 times. Nature 361, 710-712. https://doi.org/10.1038/361710a0
518 Jaffrés, J.B.D., Shields, G.A., Wallmann, K., 2007. The oxygen isotope evolution of seawater: A
519 critical review of a long-standing controversy and an improved geological water cycle
520 model for the past 3.4 billion years. Earth-Sci. Rev. 83, 83-122.
521 https://doi.org/10.1016/j.earscirev.2007.04.002
522 Janssen, N.M.M., 2003. Mediterranean Neocomian belemnites, part 2: The Berriasian-
523 Valanginian boundary in southeast Spain (Río Argos, Cañada Lengua and Tornajo). Scr.
524 Geol. 126, 121-183.

525 Jenkyns, H.C., Forster, A., Schouten, S., Sinninghe Damsté, J.S., 2004. High temperatures in the
526 late Cretaceous Arctic Ocean. Nature 432, 888-892. https://doi.org/10.1038/nature03143
527 Jenkyns, H.C., Schouten-Huibers, L., Schouten, S., Sinninghe Damsté, J.S., 2012. Warm Middle
528 Jurassic–Early Cretaceous high-latitude sea-surface temperatures from the Southern
529 Ocean. Clim. Past 8, 215-226. https://doi.org/10.5194/cp-8-215-2012
530 Kelson, J.R., Huntington, K.W., Schauer, A.J., Saenger, C., Lechler, A.R., 2017. Toward a universal
531 carbonate clumped isotope calibration: Diverse synthesis and preparatory methods
532 suggest a single temperature relationship. Geochim. Cosmochim. Acta 197, 104-131.
533 https://doi.org/10.1016/j.gca.2016.10.010
534 Kim, S.-T., O'Neil, J.R., 1997. Equilibrium and nonequilibrium oxygen isotope effects in synthetic
535 carbonates. Geochim. Cosmochim. Acta 61, 3461-3475. https://doi.org/10.1016/S0016-
536 7037(97)00169-5
537 Kim, S.-T., Mucci, A., Taylor, B.E., 2007. Phosphoric acid fractionation factors for calcite and
538 aragonite between 25 and 75 °C: Revisited. Chem. Geol. 246, 135-146.
539 https://doi.org/10.1016/j.chemgeo.2007.08.005
540 Kim, J.-H., van der Meer, J., Schouten, S., Helmke, P., Willmott, V., Sangiorgi, F., Koç, N.,
541 Hopmans, E.C., Damsté, J.S.S., 2010. New indices and calibrations derived from the
542 distribution of crenarchaeal isoprenoid tetraether lipids: Implications for past sea surface
543 temperature reconstructions. Geochim. Cosmochim. Acta 74, 4639-4654.
544 https://doi.org/10.1016/j.gca.2010.05.027
545 Klett, T.R., Wandrey, C.J., Pitman, J.K., 2011. Geology and petroleum potential of the north and
546 east margins of the Siberian Craton, north of the Arctic Circle. Arct. Pet. Geol. 35, 413-
547 431. https://doi.org/10.1144/M35.27

548 Klug, C., Schweigert, G., Fuchs, D., Kruta, I., Tischlinger, H., 2016. Adaptations to squid-style
549 high-speed swimming in Jurassic belemnitids. Biol. Lett. 12, 1-5.
550 https://doi.org/10.1098/rsbl.2015.0877
551 Kump, L.R., Pollard, D., 2008. Amplification of Cretaceous warmth by biological cloud
552 feedbacks. Science 320, 195. https://doi.org/10.1126/science.1153883
553 LeGrande, A.N., Schmidt, G.A., 2006. Global gridded data set of the oxygen isotopic
554 composition in seawater. Geophys. Res. Lett. 33, 1-5.
555 https://doi.org/10.1029/2006gl026011
556 Lindquist, S.J., 1999. The Timan-Pechora Basin province of northwest Arctic Russia; Domanik,
557 Paleozoic total petroleum system. USGS Open-File Report 99-50, 1-24.
558 https://doi.org/10.3133/ofr9950G
559 Littler, K., Robinson, S.A., Bown, P.R., Nederbragt, A.J., Pancost, R.D., 2011. High sea-surface
560 temperatures during the Early Cretaceous Epoch. Nat. Geosci. 4, 169-172.
561 https://doi.org/10.1038/ngeo1081
562 Locarnini, R.A., Mishonov, A.V., Antonov, J.I., Boyer, T.P., Garcia, H.E., Baranova, O.K., Zweng,
563 M.M., Paver, C.R., Reagan, J.R., Johnson, D.R., Hamilton, M., Seidov, D., 2013. World
564 Ocean Atlas 2013, Volume 1: Temperature.
565 Lunt, D.J., Farnsworth, A., Loptson, C., Foster, G.L., Markwick, P., apos, Brien, C.L., Pancost, R.D.,
566 Robinson, S.A., Wrobel, N., 2016. Palaeogeographic controls on climate and proxy
567 interpretation. Clim. Past 12, 1181-1198. https://doi.org/10.5194/cp-12-1181-2016
568 Marshall, J.D., 1992. Climatic and oceanographic isotopic signals from the carbonate rock
569 record and their preservation. Geol. Mag. 129, 143-160.
570 https://doi.org/10.1017/s0016756800008244
571 McArthur, J.M., Mutterlose, J., Price, G.D., Rawson, P.F., Ruffell, A., Thirlwall, M.F., 2004.
572 Belemnites of Valanginian, Hauterivian and Barremian age: Sr-isotope stratigraphy,

composition ($^{87}Sr/^{86}Sr$, $\delta^{13}C$, $\delta^{18}O$, Na, Sr, Mg), and palaeo-oceanography. Palaeogeogr. Palaeoclimatol. Palaeoecol. 202, 253-272. https://doi.org/10.1016/s0031-0182(03)00638-2

McArthur, J.M., Janssen, N.M.M., Reboulet, S., Leng, M.J., Thirlwall, M.F., van de Schootbrugge, B., 2007. Palaeotemperatures, polar ice-volume, and isotope stratigraphy (Mg/Ca, $\delta^{18}O$, $\delta^{13}C$, $^{87}Sr/^{86}Sr$): The Early Cretaceous (Berriasian, Valanginian, Hauterivian). Palaeogeogr. Palaeoclimatol. Palaeoecol. 248, 391-430. https://doi.org/10.1016/j.palaeo.2006.12.015

McConnaughey, T., 1989. ^{13}C and ^{18}O isotopic disequilibrium in biological carbonates: II. *In vitro* simulation of kinetic isotope effects. Geochim. Cosmochim. Acta 53, 163-171. https://doi.org/10.1016/0016-7037(89)90283-4

Meyer, K.W., Petersen, S.V., Lohmann, K.C., Winkelstern, I.Z., 2018. Climate of the Late Cretaceous North American Gulf and Atlantic Coasts. Cretac. Res. 89, 160-173. https://doi.org/10.1016/j.cretres.2018.03.017

Miller, K.G., 2009. Broken greenhouse windows. Nat. Geosci. 2, 465-466. https://doi.org/10.1038/ngeo563

Muehlenbachs, K., Clayton, R.N., 1976. Oxygen isotope composition of the oceanic crust and its bearing on seawater. J. Geophys. Res. 81, 4365-4369. https://doi.org/10.1029/JB081i023p04365

Muehlenbachs, K., 1998. The oxygen isotopic composition of the oceans, sediments and the seafloor. Chem. Geol. 145, 263-273. https://doi.org/10.1016/S0009-2541(97)00147-2

Mutterlose, J., Malkoc, M., Schouten, S., Sinninghe Damsté, J.S., Forster, A., 2010. TEX_{86} and stable $\delta^{18}O$ paleothermometry of early Cretaceous sediments: Implications for belemnite ecology and paleotemperature proxy application. Earth Planet. Sci. Lett. 298, 286–298. https://doi.org/10.1016/j.epsl.2010.07.043

Mutterlose, J., Malkoc, M., Schouten, S., Sinninghe Damsté, J.S., 2012. Reconstruction of vertical temperature gradients in past oceans — Proxy data from the Hauterivian–early Barremian (Early Cretaceous) of the Boreal Realm. Palaeogeogr. Palaeoclimatol. Palaeoecol. 363-364, 135-143. https://doi.org/10.1016/j.palaeo.2012.09.006

Naafs, B.D.A., Pancost, R.D., 2016. Sea-surface temperature evolution across Aptian Oceanic Anoxic Event 1a. Geology 44, 959-962. https://doi.org/10.1130/g38575.1

Nunn, E.V., Price, G.D., Gröcke, D.R., Baraboshkin, E.Y., Leng, M.J., Hart, M.B., 2010. The Valanginian positive carbon isotope event in Arctic Russia: Evidence from terrestrial and marine isotope records and implications for global carbon cycling. Cretac. Res. 31, 577-592. https://doi.org/10.1016/j.cretres.2010.07.007

O'Brien, C.L., Robinson, S.A., Pancost, R.D., Sinninghe Damsté, J.S., Schouten, S., Lunt, D.J., Alsenz, H., Bornemann, A., Bottini, C., Brassell, S.C., Farnsworth, A., Forster, A., Huber, B.T., Inglis, G.N., Jenkyns, H.C., Linnert, C., Littler, K., Markwick, P., McAnena, A., Mutterlose, J., Naafs, B.D.A., Püttmann, W., Sluijs, A., van Helmond, N.A.G.M., Vellekoop, J., Wagner, T., Wrobel, N.E., 2017. Cretaceous sea-surface temperature evolution: Constraints from TEX_{86} and planktonic foraminiferal oxygen isotopes. Earth-Sci. Rev. 172, 224-247. https://doi.org/10.1016/j.earscirev.2017.07.012

O'Connor, L.K., Robinson, S.A., Naafs, B.D.A., Jenkyns, H.C., Henson, S., Clarke, M., Pancost, R.D., 2019. Late Cretaceous temperature evolution of the southern high latitudes: a TEX_{86} perspective. Paleoceanography and Paleoclimatology 34, 436-454. https://doi.org/10.1029/2018pa003546

Passey, B.H., Henkes, G.A., 2012. Carbonate clumped isotope bond reordering and geospeedometry. Earth Planet. Sci. Lett. 351-352, 223-236. https://doi.org/10.1016/j.epsl.2012.07.021

621 Pekar, S.F., DeConto, R.M., 2006. High-resolution ice-volume estimates for the early Miocene:
622 Evidence for a dynamic ice sheet in Antarctica. Palaeogeogr. Palaeoclimatol. Palaeoecol.
623 231, 101-109. https://doi.org/10.1016/j.palaeo.2005.07.027
624 Petersen, S.V., Schrag, D.P., 2015. Antarctic ice growth before and after the Eocene-Oligocene
625 transition: New estimates from clumped isotope paleothermometry. Paleoceanography
626 30, 1305-1317. https://doi.org/10.1002/2014PA002769
627 Petersen, S.V., Tabor, C.R., Lohmann, K.C., Poulsen, C.J., Meyer, K.W., Carpenter, S.J., Erickson,
628 J.M., Matsunaga, K.K.S., Smith, S.Y., Sheldon, N.D., 2016. Temperature and salinity of the
629 Late Cretaceous Western Interior Seaway. Geology 44, 903-906.
630 https://doi.org/10.1130/g38311.1
631 Petersen, S.V., Defliese, W.F., Saenger, C., Daëron, M., Huntington, K.W., John, C.M., Kelson,
632 J.R., Coleman, A.S., Kluge, T., Olack, G.A., Schauer, A.J., Bajnai, D., Bonifacie, M.,
633 Breitenbach, S.F., Fiebig, J., Fernandez, A.B., Henkes, G.A., Hodell, D., Katz, A., Kele, S.,
634 Lohmann, K.C., Passey, B.H., Peral, M.Y., Petrizzo, D.A., Rosenheim, B.E., Tripati, A.,
635 Venturelli, R., Young, E.D., Winkelstern, I.Z., 2019. Effects of improved ^{17}O correction on
636 interlaboratory agreement in clumped isotope calibrations, estimates of mineral-specific
637 offsets, and temperature dependence of acid digestion fractionation. Geochem. Geophys.
638 Geosyst. 20, 3495-3519. https://doi.org/10.1029/2018GC008127
639 Poulsen, C.J., Pollard, D., White, T.S., 2007. General circulation model simulation of the $\delta^{18}O$
640 content of continental precipitation in the middle Cretaceous: A model-proxy
641 comparison. Geology 35, 199-202. https://doi.org/10.1130/G23343A.1
642 Price, G.D., 1999. The evidence and implications of polar ice during the Mesozoic. Earth-Sci.
643 Rev. 48, 183-210. https://doi.org/10.1016/s0012-8252(99)00048-3

644 Price, G.D., Ruffell, A.H., Jones, C.E., Kalin, R.M., Mutterlose, J., 2000. Isotopic evidence for
645 temperature variation during the early Cretaceous (late Ryazanian-mid-Hauterivian). J.
646 Geol. Soc. 157, 335-343. https://doi.org/10.1144/jgs.157.2.335
647 Price, G.D., Nunn, E.V., 2010. Valanginian isotope variation in glendonites and belemnites from
648 Arctic Svalbard: Transient glacial temperatures during the Cretaceous greenhouse.
649 Geology 38, 251-254. https://doi.org/10.1130/g30593.1
650 Price, G.D., Passey, B.H., 2013. Dynamic polar climates in a greenhouse world: Evidence from
651 clumped isotope thermometry of Early Cretaceous belemnites. Geology 41, 923-926.
652 https://doi.org/10.1130/g34484.1
653 Price, G.D., Hart, M.B., Wilby, P.R., Page, K.N., 2015. Isotopic analysis of Jurassic (Callovian)
654 mollusks from the Christian Malford lagerstätte (UK): Implications for ocean water
655 temperature estimates based on belemnoids. Palaios 30, 645-654.
656 https://doi.org/10.2110/palo.2014.106
657 Price, G.D., Janssen, N.M.M., Martinez, M., Company, M., Vandevelde, J.H., Grimes, S.T., 2018.
658 A high-resolution belemnite geochemical analysis of Early Cretaceous (Valanginian-
659 Hauterivian) environmental and climatic perturbations. Geochem. Geophys. Geosyst. 19,
660 3832-3843. https://doi.org/10.1029/2018gc007676
661 Pucéat, E., Lecuyer, C., Sheppard, S.M.F., Dromart, G., Reboulet, S., Grandjean, P., 2003.
662 Thermal evolution of Cretaceous Tethyan marine waters inferred from oxygen isotope
663 composition of fish tooth enamels. Paleoceanography 18, 1029.
664 https://doi.org/10.1029/2002pa000823
665 Railsback, L.B., Anderson, T.F., Ackerly, S.C., Cisne, J.L., 1989. Paleoceanographic modeling of
666 temperature-salinity profiles from stable isotopic data. Paleoceanography 4, 585-591.
667 https://doi.org/10.1029/PA004i005p00585

668 Rawson, P.F., 1973. Lower Cretaceous (Ryazanian-Barremian) marine connections and
669 cephalopod migrations between the Tethyan and Boreal Realms, in: Casey, R., Rawson,
670 P.F. (Eds.), The Boreal Lower Cretaceous. Seel House Press, Liverpool, pp. 131-144.
671 Reboulet, S., Szives, O., Aguirre-Urreta, B., Barragán, R., Company, M., Frau, C., Kakabadze,
672 M.V., Klein, J., Moreno-Bedmar, J.A., Lukeneder, A., Pictet, A., Ploch, I., Raisossadat, S.N.,
673 Vašíček, Z., Baraboshkin, E.J., Mitta, V.V., 2018. Report on the 6th International Meeting
674 of the IUGS Lower Cretaceous Ammonite Working Group, the Kilian Group (Vienna,
675 Austria, 20th August 2017). Cretac. Res. 91, 100-110.
676 https://doi.org/10.1016/j.cretres.2018.05.008
677 Reicherter, K., Wiedmann, J., Herbin, J.P., 1996. Distribution of organic-rich sediments in
678 Subbetic sections during the Aptian-Turonian (Betic Cordillera, Southern Spain). Rev. Soc.
679 Geol. Esp. 9, 75-88.
680 Rogov, M.A., Ershova, V.B., Shchepetova, E.V., Zakharov, V.A., Pokrovsky, B.G., Khudoley, A.K.,
681 2017. Earliest Cretaceous (late Berriasian) glendonites from Northeast Siberia revise the
682 timing of initiation of transient Early Cretaceous cooling in the high latitudes. Cretac. Res.
683 71, 102-112. https://doi.org/10.1016/j.cretres.2016.11.011
684 Ryb, U., Eiler, J.M., 2018. Oxygen isotope composition of the Phanerozoic ocean and a possible
685 solution to the dolomite problem. Proc. Natl. Acad. Sci. U.S.A. 115, 6602-6607.
686 https://doi.org/10.1073/pnas.1719681115
687 Sælen, G., 1989. Diagenesis and construction of the belemnite rostrum. Palaeontology 32, 765-
688 797.
689 Sagoo, N., Valdes, P., Flecker, R., Gregoire, L.J., 2013. The Early Eocene equable climate
690 problem: Can perturbations of climate model parameters identify possible solutions?
691 Philos. T. R. Soc. A 371, 20130123. https://doi.org/10.1098/rsta.2013.0123

692 Schmidt, G.A., Mysak, L.A., 1996. Can increased poleward oceanic heat flux explain the warm
693 Cretaceous climate? Paleoceanography 11, 579-593. https://doi.org/10.1029/96pa01851
694 van de Schootbrugge, B., Föllmi, K.B., Bulot, L.G., Burns, S.J., 2000. Paleoceanographic changes
695 during the early Cretaceous (Valanginian-Hauterivian): evidence from oxygen and carbon
696 stable isotopes. Earth Planet. Sci. Lett. 181, 15-31. https://doi.org/10.1016/S0012-
697 821X(00)00194-1
698 Scotese, C.R., 2014. Atlas of Early Cretaceous Paleogeographic Maps, PALEOMAP Atlas for
699 ArcGIS, volume 2, The Cretaceous, Maps 23-31, Mollweide Projection, Evanston, IL, USA.
700 Shackleton, N.J., Kennett, J.P., 1975. Paleotemperature history of the Cenozoic and the
701 initiation of antarctic glaciation: oxygen and carbon isotope analyses in DSDP sites 277,
702 279, and 281. Deep Sea Drilling Project Initial Reports 29, 743-755.
703 https://doi.org/10.2973/dsdp.proc.29.117.1975
704 Shulgina, N.I., Burdykina, M.D., Basov, V.A., Arhus, N., 1994. Distribution of ammonites,
705 foraminifera and dinoflagellate cysts in the Lower Cretaceous reference sections of the
706 Khatanga Basin, and Boreal Valanginian biogeography. Cretac. Res. 15, 1-16.
707 https://doi.org/10.1006/cres.1994.1001
708 Słowakiewicz, M., Tucker, M.E., Vane, C.H., Harding, R., Collins, A., Pancost, R.D., 2015. Shale-
709 gas potential of the mid-Carboniferous Bowland-Hodder Unit in the Cleveland Basin
710 (Yorkshire), central Britain. J. Pet. Geol 38, 59-75. https://doi.org/10.1111/jpg.12598
711 Spicer, R.A., Ahlberg, A., Herman, A.B., Hofmann, C.-C., Raikevich, M., Valdes, P.J., Markwick,
712 P.J., 2008. The Late Cretaceous continental interior of Siberia: A challenge for climate
713 models. Earth Planet. Sci. Lett. 267, 228-235. https://doi.org/10.1016/j.epsl.2007.11.049
714 Spicer, R.A., Herman, A.B., 2010. The Late Cretaceous environment of the Arctic: A quantitative
715 reassessment based on plant fossils. Palaeogeogr. Palaeoclimatol. Palaeoecol. 295, 423-
716 442. https://doi.org/10.1016/j.palaeo.2010.02.025

717 Stevens, K., Mutterlose, J., Schweigert, G., 2014. Belemnite ecology and the environment of the
718 Nusplingen Plattenkalk (Late Jurassic, southern Germany): Evidence from stable isotope
719 data. Lethaia 47, 512-523. https://doi.org/10.1111/let.12076
720 Super, J.R., Chin, K., Pagani, M., Li, H., Tabor, C., Harwood, D.M., Hull, P.M., 2018. Late
721 Cretaceous climate in the Canadian Arctic: Multi-proxy constraints from Devon Island.
722 Palaeogeogr. Palaeoclimatol. Palaeoecol. 504, 1-22.
723 https://doi.org/10.1016/j.palaeo.2018.03.004
724 Tarduno, J.A., Brinkman, D.B., Renne, P.R., Cottrell, R.D., Scher, H., Castillo, P., 1998. Evidence
725 for extreme climatic warmth from Late Cretaceous Arctic vertebrates. Science 282, 2241-
726 2244. https://doi.org/10.1126/science.282.5397.2241
727 Tierney, J.E., Tingley, M.P., 2014. A Bayesian, spatially-varying calibration model for the TEX_{86}
728 proxy. Geochim. Cosmochim. Acta 127, 83-106.
729 https://doi.org/10.1016/j.gca.2013.11.026
730 Upchurch, G.R., Kiehl, J., Shields, C., Scherer, J., Scotese, C., 2015. Latitudinal temperature
731 gradients and high-latitude temperatures during the latest Cretaceous: Congruence of
732 geologic data and climate models. Geology 43, 683-686.
733 https://doi.org/10.1130/g36802.1
734 Veizer, J., 1974. Chemical diagenesis belemnite shells possible consequences for
735 paleotemperature determinations. Neues Jahrb. Geol. Palaontol. Abhand. 147, 91-111.
736 Veizer, J., Prokoph, A., 2015. Temperatures and oxygen isotopic composition of Phanerozoic
737 oceans. Earth-Sci. Rev. 146, 92-104. https://doi.org/10.1016/j.earscirev.2015.03.008
738 Vickers, M.L., Price, G.D., Jerrett, R.M., Watkinson, M., 2016. Stratigraphic and geochemical
739 expression of Barremian–Aptian global climate change in Arctic Svalbard. Geosphere 12,
740 1594-1605. https://doi.org/10.1130/ges01344.1

741 Vickers, M.L., Bajnai, D., Price, G.D., Linckens, J., Fiebig, J., 2019. Southern high latitude warmth
742 during Jurassic–Cretaceous: New evidence from clumped isotope thermometry. Geology
743 47, 724-728. https://doi.org/10.1130/G46263.1
744 Voigt, S., Wilmsen, M., Mortimore, R.N., Voigt, T., 2003. Cenomanian palaeotemperatures
745 derived from the oxygen isotopic composition of brachiopods and belemnites: evaluation
746 of Cretaceous palaeotemperature proxies. Int. J. Earth Sci. 92, 285-299.
747 https://doi.org/10.1007/s00531-003-0315-1
748 Wacker, U., Fiebig, J., Tödter, J., Schöne, B.R., Bahr, A., Friedrich, O., Tütken, T., Gischler, E.,
749 Joachimski, M.M., 2014. Empirical calibration of the clumped isotope paleothermometer
750 using calcites of various origins. Geochim. Cosmochim. Acta 141, 127-144.
751 https://doi.org/10.1016/j.gca.2014.06.004
752 Wallmann, K., 2004. Impact of atmospheric CO_2 and galactic cosmic radiation on Phanerozoic
753 climate change and the marine $\delta^{18}O$ record. Geochem. Geophys. Geosyst. 5, 1-29.
754 https://doi.org/10.1029/2003gc000683
755 Wang, Y., Huang, C., Sun, B., Quan, C., Wu, J., Lin, Z., 2014. Paleo-CO_2 variation trends and the
756 Cretaceous greenhouse climate. Earth-Sci. Rev. 129, 136-147.
757 https://doi.org/10.1016/j.earscirev.2013.11.001
758 White, T., Gonzalez, L., Ludvigson, G., Poulsen, C., 2001. Middle Cretaceous greenhouse
759 hydrologic cycle of North America. Geology 29, 363-366. https://doi.org/10.1130/0091-
760 7613(2001)029<0363:Mcghco>2.0.Co;2
761 Wierzbowski, H., Rogov, M.A., Matyja, B.A., Kiselev, D., Ippolitov, A., 2013. Middle–Upper
762 Jurassic (Upper Callovian–Lower Kimmeridgian) stable isotope and elemental records of
763 the Russian Platform: Indices of oceanographic and climatic changes. Glob. Planet.
764 Change 107, 196-212. https://doi.org/10.1016/j.gloplacha.2013.05.011

765 Wierzbowski, H., Bajnai, D., Wacker, U., Rogov, M.A., Fiebig, J., Tesakova, E.M., 2018. Clumped
766 isotope record of salinity variations in the Subboreal Province at the middle–late Jurassic
767 transition. Glob. Planet. Change 167, 172-189.
768 https://doi.org/10.1016/j.gloplacha.2018.05.014
769 Witkowski, C.R., Weijers, J.W.H., Blais, B., Schouten, S., Sinninghe Damsté, J.S., 2018. Molecular
770 fossils from phytoplankton reveal secular pCO_2 trend over the Phanerozoic. Sci. Adv. 4,
771 eaat4556. https://doi.org/10.1126/sciadv.aat4556
772 Young, A., Flament, N., Maloney, K., Williams, S., Matthews, K., Zahirovic, S., Müller, R.D., 2019.
773 Global kinematics of tectonic plates and subduction zones since the late Paleozoic Era.
774 Geosci. Front. 10, 989-1013. https://doi.org/10.1016/j.gsf.2018.05.011
775 Zakharov, V.A., Bogomolov, Y.I., Il'ina, V.I., Konstantinov, A.G., Kurushin, N.I., Lebedeva, N.K.,
776 Meledina, S.V., Nikitenko, B.L., Sobolev, E.S., Shurygin, B.N., 1997. Boreal zonal standard
777 and biostratigraphy of the Siberian Mesozoic. Russ. Geol. Geophys. 38, 965-993.
778 Zeebe, R.E., 1999. An explanation of the effect of seawater carbonate concentration on
779 foraminiferal oxygen isotopes. Geochim. Cosmochim. Acta 63, 2001-2007.
780 https://doi.org/10.1016/S0016-7037(99)00091-5
781 Zeebe, R.E., 2001. Seawater pH and isotopic paleotemperatures of Cretaceous ocean.
782 Palaeogeogr. Palaeoclimatol. Palaeoecol. 170, 49-57. https://doi.org/10.1016/S0031-
783 0182(01)00226-7
784 Zhou, J., Poulsen, C.J., Pollard, D., White, T.S., 2008. Simulation of modern and middle
785 Cretaceous marine $\delta^{18}O$ with an ocean-atmosphere general circulation model.
786 Paleoceanography 23, PA3223. https://doi.org/10.1029/2008pa001596
787 Zhu, J., Poulsen, C.J., Tierney, J.E., 2019. Simulation of Eocene extreme warmth and high climate
788 sensitivity through cloud feedbacks. Sci. Adv. 5, eaax1874.
789 https://doi.org/10.1126/sciadv.aax1874
790

Figures

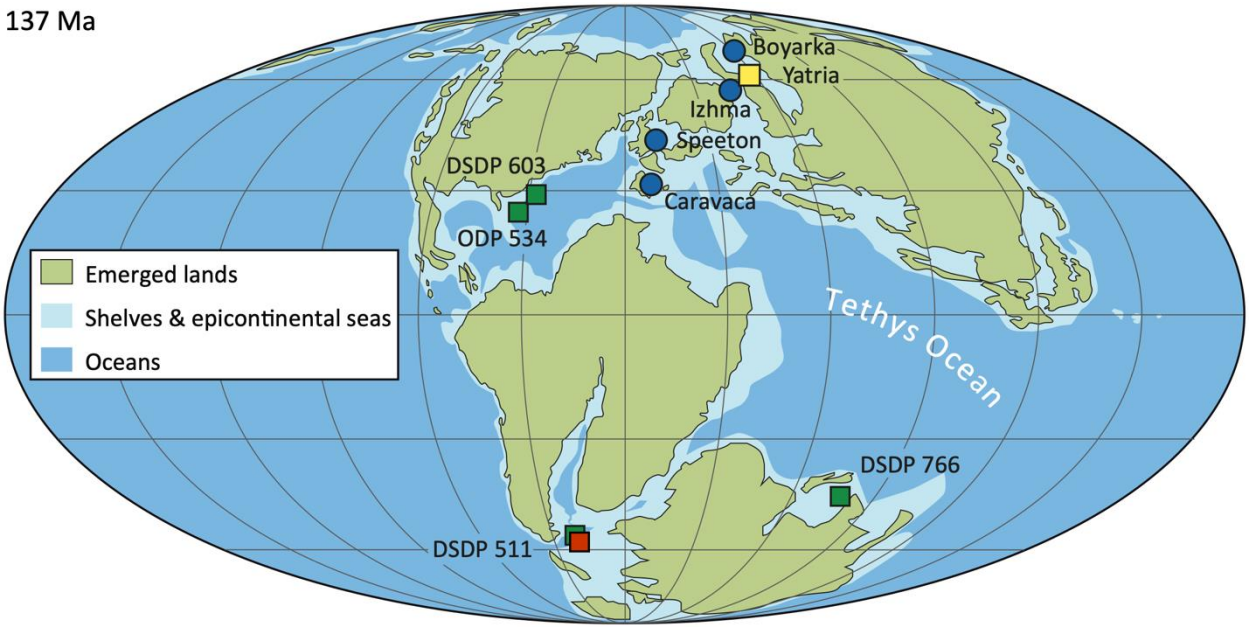

Fig. 1. Early Cretaceous palaeogeographic reconstruction with locations of the discussed study sites. Map modified after Scotese (2014). Blue circles = data from this study; green squares = location of published Early Cretaceous TEX_{86} data (Littler et al. 2011; Jenkyns et al. 2012). The locations of additional published Δ_{47}-based temperature data are marked with a yellow square (Price and Passey, 2013) and a red square (Vickers et al. 2019). The palaeolatitude estimates are consistent with Young et al. (2019) that are used for Figs 3 and 4.

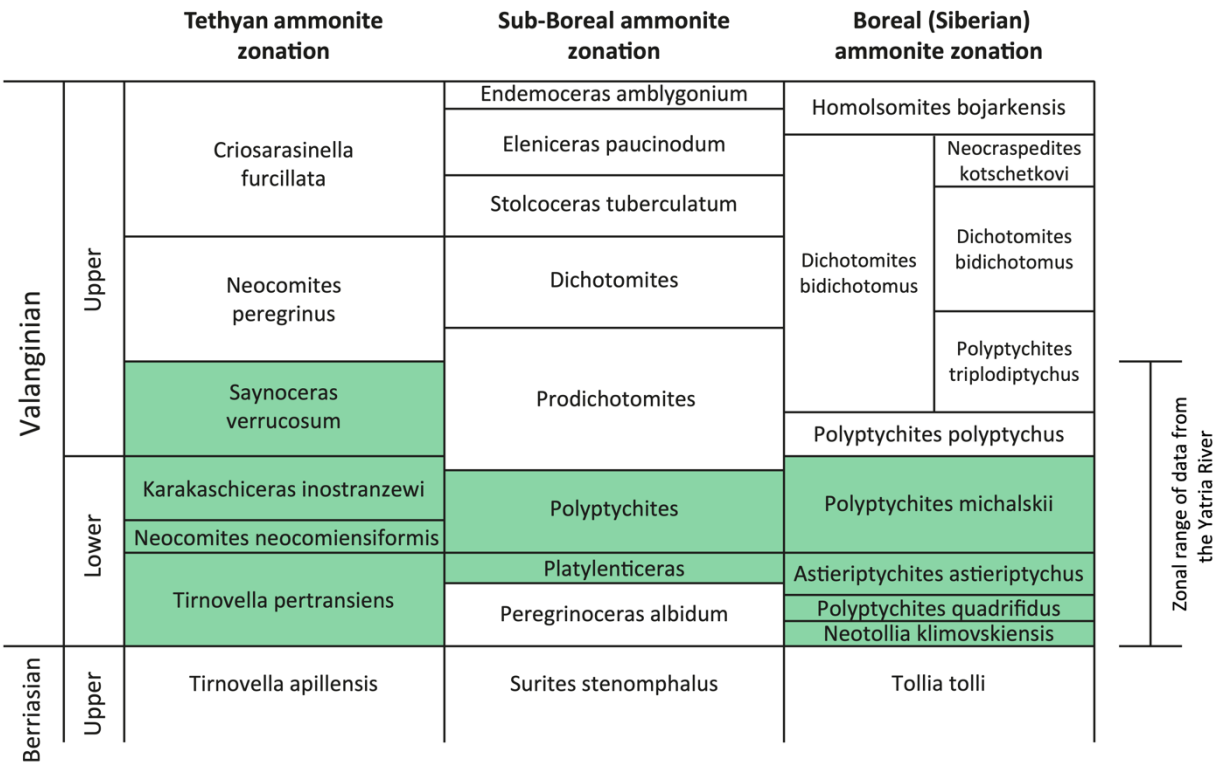

Fig. 2. Biostratigraphic correlation of the Early Cretaceous Tethyan (Reboulet et al., 2018) sub-Boreal and Boreal (Gradstein et al. 2012; Nunn et al. 2010; Shulgina et al., 1994; Zakharov et al., 1997; Baraboshkin, 2004) ammonite schemes. The green shaded area indicates the position of sampled Valanginian zones for Tethyan (Caravaca, Spain), Sub-Boreal (Speeton), and Boreal sites (Khatanga Basin and Pechora Basin). The ammonite range of additional Valanginian Δ_{47} data from the Yatria River is shown (Price and Passey 2013). Early Cretaceous southern high latitude data shown on Figs 3 and 4 have less constrained biostratigraphy (Vickers et al., 2019).

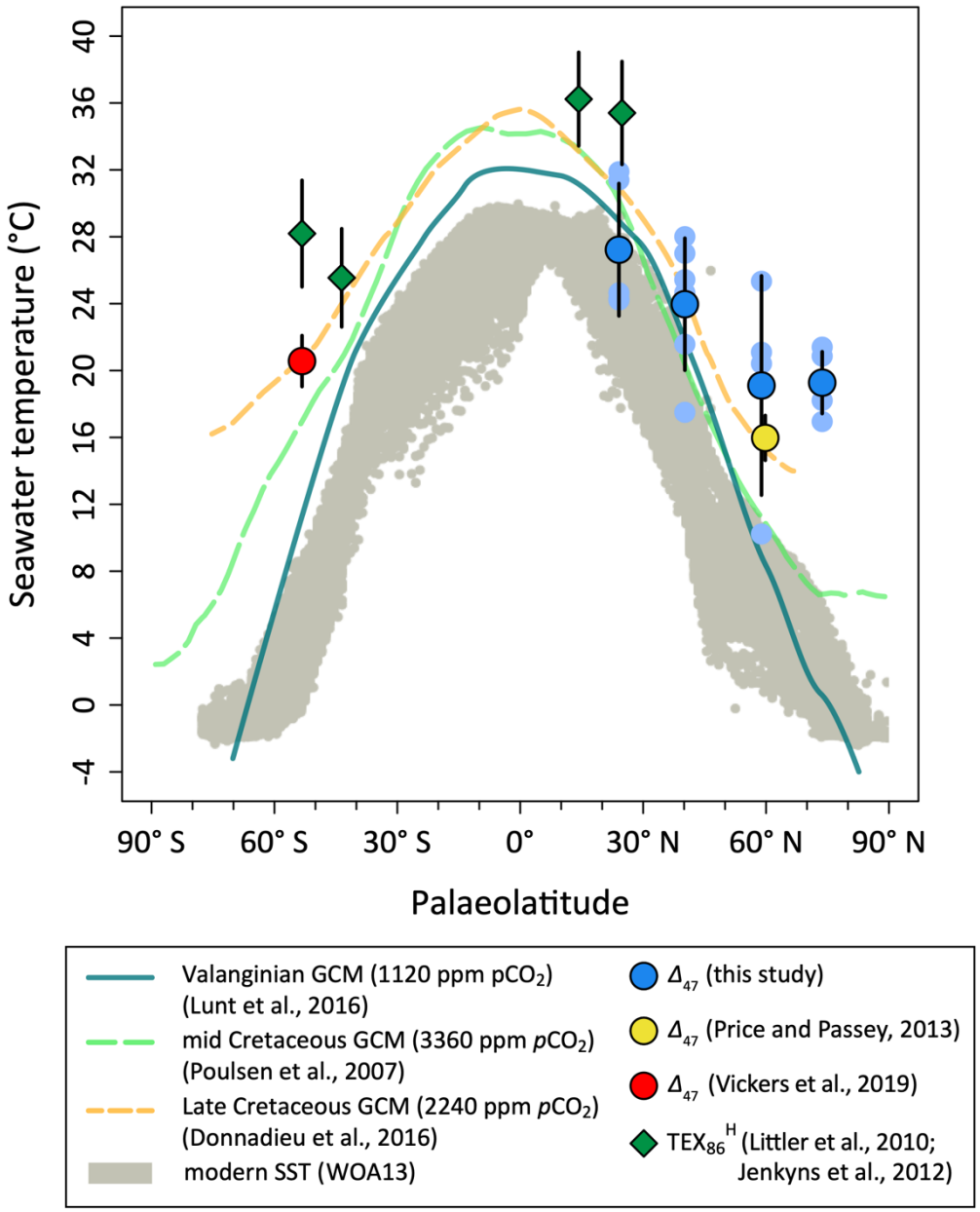

806 **Fig. 3.** Early Cretaceous (Valanginian) meridional temperature reconstruction. Mean annual
807 surface temperature observations from the World Ocean Atlas (Locarnini et al., 2013).
808 Valanginian TEX_{86} temperatures (Littler et al., 2011) were recalculated using the TEX_{86}^{H}
809 calibration (Kim et al., 2010). Dark blue circles show mean Δ_{47}-based temperatures from this
810 study with ± uncertainties corresponding to the standard deviation from individual belemnites
811 (light blue circles). Additional Δ_{47} data of Vickers et al., (2019) (for the Early Cretaceous) and
812 Price and Passey (2013) (Valanginian) were converted to temperatures using the synthetic
813 calcite calibration of Petersen et al. (2019). Early Cretaceous data are compared with sea
814 surface temperatures from the Early Cretaceous (Valanginian) GCM with 4x pre-industrial pCO_2

(Lunt et al., 2016) a mid-Cretaceous GCM with 12x pre-industrial pCO_2 (Poulsen et al., 2007) and a Late Cretaceous GCM with 8x pre-industrial pCO_2 (Donnadieu et al., 2016). Thermal gradients of the simulations have been calculated from an average over the longitudes including the South Atlantic sector and the Tethyan area (see Donnadieu et al., 2016). A version of this plot where Δ_{47}-based temperatures are calculated using the Wacker et al. (2014) equation is shown in the Supplementary Information.

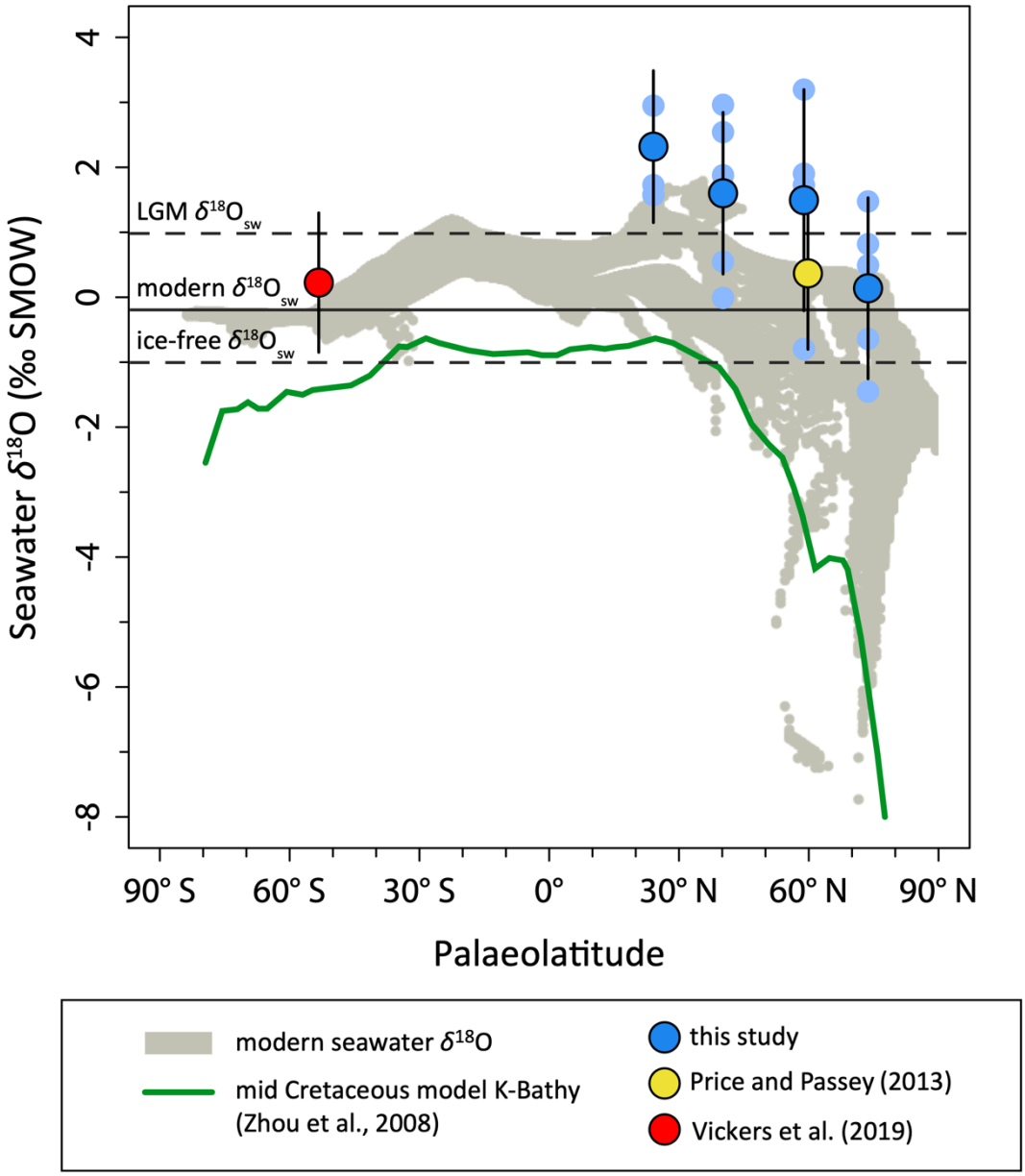

821 **Fig. 4.** Early Cretaceous (Valanginian) meridional seawater oxygen isotope gradient. Modern
822 gridded mean annual $\delta^{18}O_{sw}$ values from LeGrande and Schmidt (2006). $\delta^{18}O_{sw}$ (‰ SMOW)
823 calculated using the Kim and O'Neil (1997) equation (see Supplementary Figure 2 for Coplen
824 (2007) equation) with additional Valanginian data derived from Price and Passey (2013) and
825 Vickers et al. (2019). Dark blue circles are mean estimates and ± uncertainties are standard
826 deviations. Light blue circles are estimates from individual belemnites. Modelled mid
827 Cretaceous mean annual zonal average of $\delta^{18}O_{sw}$ after Zhou, et al. (2008).

828 **Table 1.** Clumped and bulk isotopic composition of Early Cretaceous belemnites

Sample	Taxonomy	Location	N	$\delta^{13}C$ (‰ VPDB)	$\delta^{18}O$ (‰ VPDB)	$\Delta_{47\ (RFAC)}$ (‰)	Temperature (°C)	$\delta^{18}O_{sw}$ (‰ SMOW) Coplen (2007)	$\delta^{18}O_{sw}$ (‰ SMOW) Kim and O'Neil (1997)
KH18-10.50	*Acroteuthis* sp.	Boyarka	5	0.22	-1.55	0.707 (±0.005)	19 (±1)	-2.1 (±0.3)	-0.6 (±0.3)
KH18-11.20	indet.	Boyarka	5	1.12	-0.48	0.701 (±0.006)	21 (±2)	-0.6 (±0.4)	0.8 (±0.4)
KH18-27.00	*Lagonibelus* sp.	Boyarka	6	0.96	0.03	0.713 (±0.006)	17 (±2)	-0.9 (±0.4)	0.5 (±0.4)
KH18-2.85	indet.	Boyarka	5	0.38	0.07	0.699 (±0.009)	21 (±3)	0.0 (±0.6)	1.5 (±0.6)
KH18-7.10	*Pachyteuthis* sp.	Boyarka	5	0.60	-2.19	0.709 (±0.007)	18 (±2)	-2.9 (±0.5)	-1.5 (±0.5)
YCL214-031	*Berriasibelus* sp.	Caravaca	6	-1.25	-0.57	0.670 (±0.012)	32 (±5)	1.4 (±0.9)	2.9 (±0.9)
YG14-015	*Duvalia* sp.	Caravaca	3	0.50	0.37	0.671 (±0.007)	31 (±3)	2.3 (±0.5)	3.8 (±0.5)
YP14-005	*Hibolithes* sp.	Caravaca	5	1.74	-0.41	0.691 (±0.013)	24 (±4)	0.1 (±0.9)	1.6 (±0.9)
YP14-001	*Duvalia* cf. *lata*	Caravaca	6	-0.29	-0.50	0.690 (±0.009)	25 (±3)	0.1 (±0.6)	1.6 (±0.7)
YP14-014	*Duvalia binervia*	Caravaca	4	0.95	-0.27	0.691 (±0.009)	24 (±3)	0.3 (±0.6)	1.7 (±0.6)
PC7-B1	*Pachyteuthis* sp.	Izhma	7	-0.49	0.21	0.735 (±0.004)	10 (±1)	-2.1 (±0.3)	-0.8 (±0.3)
PC7-B2	*Pachyteuthis* sp.	Izhma	6	0.19	0.56	0.700 (±0.003)	21 (±1)	0.5 (±0.2)	1.9 (±0.2)

PC9-G23	indet.	Izhma	5	-0.79	0.52	0.702 (±0.007)	20 (±2)	0.3 (±0.5)	1.7 (±0.5)
PC9-G8	*Acroteuthis* sp.	Izhma	7	1.16	0.98	0.688 (±0.005)	25 (±2)	1.7 (±0.3)	3.2 (±0.3)
D2E	*Acroteuthis* sp.	Speeton	2	-0.46	-0.36	0.690 (±0.007)	25 (±2)	0.3 (±0.5)	1.7 (±0.5)
D3D	*Acroteuthis* sp.	Speeton	2	-0.09	-0.21	0.680 (±0.020)	28 (±7)	1.1 (±1.4)	2.5 (±1.4)
D4A	*Acroteuthis* sp.	Speeton	6	0.51	0.41	0.683 (±0.004)	27 (±1)	1.5 (±0.3)	3.0 (±0.3)
SP 1181	*Acroteuthis* sp.	Speeton	5	-0.12	-0.60	0.711 (±0.004)	18 (±1)	-1.4 (±0.3)	0.0 (±0.3)
SP 1297	*Acroteuthis* sp.	Speeton	4	0.60	-0.89	0.699 (±0.005)	22 (±2)	-0.9 (±0.3)	0.5 (±0.3)
SP 1S22C	*Acroteuthis* sp.	Speeton	5	0.60	-0.36	0.688 (±0.005)	25 (±2)	0.4 (±0.3)	1.9 (±0.3)

The standard error of the carbonate $\delta^{13}C$ and $\delta^{18}O$ values is 0.01‰. The ± uncertainty in the $\Delta_{47\ (RFAC)}$ values represents the (external) standard error of 2–7 replicate analyses, multiplied by the *t*-value that corresponds to the number of replicates (68.2% confidence interval). The $\Delta_{47\ (RFAC)}$ values were converted to temperatures using synthetic calcite calibration (Petersen et al., 2019) as discussed in the text (Data S1). The error in the calculated temperatures and $\delta^{18}O_{sw}$ correspond to the standard error of the $\Delta_{47\ (RFAC)}$ values.

Table 2. Mean seawater temperatures and $\delta^{18}O_{sw}$ for the locations in this study.

Location	Palaeolatitude	Number of belemnites	Mean seawater temperature (°C)	Mean $\delta^{18}O_{sw}$ (‰ SMOW) Coplen (2007)	Mean $\delta^{18}O_{sw}$ (‰ SMOW) Kim and O'Neil (1997)
Caravaca	24° N	5	27 (±4)	0.8 (±1.1)	2.3 (±1.2)
Speeton	40° N	6	24 (±4)	0.1 (±1.2)	1.6 (±1.2)
Izhma	59° N	4	19 (±7)	0.1 (±1.7)	1.5 (±1.7)
Boyarka	74° N	5	19 (±2)	-1.3 (±1.4)	0.1 (±1.4)

The ± uncertainties for the mean temperatures are calculated using the standard deviation of the $\Delta_{47\,(RFAC)}$ values of the individual belemnites (Table 1). This uncertainty was combined with the standard deviation of the $\delta^{18}O$ values of the individual belemnites to calculate the ± uncertainties for the mean $\delta^{18}O_{sw}$ values. Palaeolatitude estimates are from Young et al. (2019).